Initial data for Einstein's equations with superposed gravitational waves

Harald P. Pfeiffer,[1] Lawrence E. Kidder,[2] Mark A. Scheel,[1] and Deirdre Shoemaker[3]

[1]*Theoretical Astrophysics 130-33, California Institute of Technology, Pasadena, California 91125, USA*
[2]*Center for Radiophysics and Space Research, Cornell University, Ithaca, New York 14853, USA*
[3]*Department of Physics and Institute of Gravitational Physics and Geometry, Penn State University,
University Park, Pennsylvania 16802, USA*

A method is presented to construct initial data for Einstein's equations as a superposition of a gravitational wave perturbation on an arbitrary stationary background spacetime. The method combines the conformal thin sandwich formalism with linear gravitational waves, and allows detailed control over characteristics of the superposed gravitational wave like shape, location and propagation direction. It is furthermore fully covariant with respect to spatial coordinate changes and allows for very large amplitude of the gravitational wave.

I. INTRODUCTION

Vacuum spacetimes which are perturbed away from stationary solutions of Einstein's equations are interesting in many different aspects. Using perturbations of flat space, one can examine (critical) collapse to black holes [1,2], or investigate nonlinear interaction between gravitational waves. Perturbed black holes are expected to be produced by astrophysical events like binary black hole coalescence. Detailed understanding of the behavior of perturbed black holes, including the nonlinear regime, will be important for analyzing data from gravitational wave detectors like GEO, LIGO, TAMA and VIRGO. Numerical evolutions are the only known avenue to analyze Einstein's equation in general, three-dimensional, nonlinear situations. Moreover, nonstationary spacetimes without black holes or with just one perturbed black hole provide important test beds and benchmarks for numerical evolution codes in a computational setting much simpler than a full binary black hole evolution.

Such numerical evolutions require initial data representing perturbed spacetimes. Historically, Brill waves [3] are the most widely used approach to construct perturbations of Minkowski space with such a nonstationary component (e.g., [4–7]). They are based on certain simplifying assumptions, and allow for variations of the gravitational wave perturbation through a freely specifiable function, commonly called q. Brill's idea has also been generalized to three dimensions and to black hole spacetimes (e.g., [8–13]). All of these authors continue to encode the perturbation in a function q. It appears that, generally, this function is chosen rather *ad hoc*, its purpose mainly being to perturb the spacetime in *some* way. While every (nonzero) choice for q leads to a perturbed initial data set, it is not clear what properties the perturbation has, nor how to control these properties. Given that q is often chosen to be bell shaped (e.g., a Gaussian), it seems likely that the resulting perturbation is some vaguely localized lump of energy, rather than, say, a coherently traveling wave. Part of the motiva-

tion to use Brill waves was certainly that they lead to fairly simple equations which are easy to solve numerically. Since elliptic solvers have matured considerably over the last years (e.g., [14–17]), computational complexity is no longer a serious issue, and one is free to look for more general approaches, with easier to interpret properties of the resulting initial data sets.

An obvious starting point are linearized gravitational waves [18], which then are incorporated into the solution of the initial value problem [2,19–21]. Here, we continue along this line of thought, and propose a conceptually very simple method, which combines linear gravitational waves with the conformal thin sandwich formalism [22]. Our basic idea is to build the linear gravitational wave into the free data for the conformal thin sandwich equations. The method allows superposition of an arbitrary linear gravitational wave onto an arbitrary background spacetime. The constructed data sets retain, at least qualitatively, the properties of the underlying linear gravitational wave. Thus, properties of the perturbation to be inserted in the initial data set can be controlled easily by selecting the appropriate underlying linear gravitational wave solution.

In Sec. II, we present the method and discuss its relationship to previous work [2,19–21]. As an illustration we superpose, in Sec. III, quadrupolar gravitational waves on Minkowski space and on a Schwarzschild black hole. We close with a discussion in Sec. IV.

II. METHOD

Employing the usual 3+1 decomposition of Einstein's equations [23,24], the spacetime metric is written as

$$^{(4)}ds^2 = -N^2 dt^2 + g_{ij}(dx^i + \beta^i dt)(dx^j + \beta^j dt), \quad (1)$$

where g_{ij} represents the spatial metric on $t = $ const. hypersurfaces, and N and β^i denote the lapse-function and shift vector, respectively. The extrinsic curvature, K_{ij}, is defined by $K = -\frac{1}{2} \perp \mathcal{L}_n^{(4)}\mathbf{g}$, where $^{(4)}\mathbf{g}$ represents the spacetime

metric, n the future-pointing unit normal to the hypersurface, and $\perp$ the projection operator into the hypersurface. Einstein's equations then split into evolution equations,

$$(\partial_t - \mathcal{L}_\beta)g_{ij} = -2NK_{ij}, \tag{2}$$

$$(\partial_t - \mathcal{L}_\beta)K_{ij} = N(R_{ij} - 2K_{ik}K_j^k + KK_{ij}) - \nabla_i\nabla_j N, \tag{3}$$

and constraint equations,

$$R + K^2 - K_{ij}K^{ij} = 0, \tag{4}$$

$$\nabla_j(K^{ij} - g^{ij}K) = 0. \tag{5}$$

Here, ∇_i is the covariant derivative compatible with g_{ij}, $\mathcal{L}$ represents the Lie-derivative, and R_{ij} denotes the Ricci tensor of g_{ij}. Furthermore, R and K denote the traces of the Ricci tensor and the extrinsic curvature, respectively, and we have assumed vacuum. Initial data for Einstein's equations consists of (g_{ij}, K^{ij}). The difficulty in constructing such data lies in the requirement that the Hamiltonian and momentum constraints, Eqs. (4) and (5), must be satisfied.

One widely used formalism for constructing initial data is the conformal thin sandwich approach [22,25]. It is based on two neighboring hypersurfaces, their conformal three-geometries, and the instantaneous time-derivative of the conformal three-geometry. One introduces a conformal spatial metric $\tilde{g}_{ij}$, related to the physical spatial metric by

$$g_{ij} = \psi^4 \tilde{g}_{ij}, \tag{6}$$

where ψ is called the conformal factor. To construct initial data, one chooses the conformal metric $\tilde{g}_{ij}$, its time-derivative

$$\tilde{u}_{ij} = \partial_t \tilde{g}_{ij}, \tag{7}$$

as well as the trace of the extrinsic curvature K and the conformal lapse $\tilde{N} = \psi^{-6}N$. We note that $\tilde{u}_{ij}$ must be traceless, $\tilde{u}_{ij}\tilde{g}^{ij} = 0$. Having made these choices, the Hamiltonian and momentum constraints take the form

$$\tilde{\nabla}^2\psi - \frac{1}{8}\psi\tilde{R} - \frac{1}{12}\psi^5 K^2 + \frac{1}{8}\psi^{-7}\tilde{A}_{ij}\tilde{A}^{ij} = 0, \tag{8}$$

$$\tilde{\nabla}_j\left[\frac{1}{2\tilde{N}}(\tilde{\mathbb{L}}\beta)^{ij}\right] - \tilde{\nabla}_j\left(\frac{1}{2\tilde{N}}\tilde{u}^{ij}\right) - \frac{2}{3}\psi^6\tilde{\nabla}^i K = 0. \tag{9}$$

Here, $\tilde{\nabla}_i$ and $\tilde{R}$ are the covariant derivative compatible with $\tilde{g}_{ij}$ and the trace of the Ricci tensor of $\tilde{g}_{ij}$, respectively, $\tilde{\mathbb{L}}$ denotes the longitudinal operator,

$$(\tilde{\mathbb{L}}\beta)^{ij} = \tilde{\nabla}^i\beta^j + \tilde{\nabla}^j\beta^i - \frac{2}{3}\tilde{g}^{ij}\tilde{\nabla}_k\beta^k, \tag{10}$$

and $\tilde{A}^{ij}$ is defined as

$$\tilde{A}^{ij} = \frac{1}{2\tilde{N}}\left((\tilde{\mathbb{L}}\beta)^{ij} - \tilde{u}^{ij}\right). \tag{11}$$

Equations (8) and (9) are elliptic equations for the conformal factor ψ and the shift β^i. After solving these equations for ψ and β^i, the physical initial data is given by Eq. (6) and by

$$K^{ij} = \psi^{-10}\tilde{A}^{ij} + \frac{1}{3}g^{ij}K. \tag{12}$$

Instead of specifying $\tilde{N}$ as part of the free data one can also set $\partial_t K$. It is well known that this leads to an elliptic condition for the lapse-function (e.g., [25–27]):

$$\tilde{\nabla}^2(\tilde{N}\psi^7) - (\tilde{N}\psi^7)\left(\frac{1}{8}\tilde{R} + \frac{5}{12}\psi^4 K^2 + \frac{7}{8}\psi^{-8}\tilde{A}_{ij}\tilde{A}^{ij}\right)$$
$$= -\psi^5(\partial_t K - \beta^k\partial_k K). \tag{13}$$

The second ingredient into the construction of perturbed initial data is *linear* gravitational waves. In linearized gravity [18], the spacetime metric is written as

$$^{(4)}\mathbf{g}_{\mu\nu} = \eta_{\mu\nu} + Ah_{\mu\nu}, \tag{14}$$

where $\eta_{\mu\nu}$ is the Minkowski-metric, $A \ll 1$ a constant, and $h_{\mu\nu} = \mathcal{O}(1)$ the linear gravitational wave. (We separate the amplitude A from $h_{\mu\nu}$ for later convenience.) In transverse-traceless gauge [18], $h_{\mu\nu}$ is purely spatial, $h_{\mu 0} = h_{0\mu} = 0$, transverse with respect to Minkowski space, $\nabla^i h_{ij} = 0$, and traceless, $\eta^{ij}h_{ij} = 0$. To first order in the amplitude A, Einstein's equations reduce to

$$\Box h_{ij} = 0, \tag{15}$$

where $\Box$ is the Minkowski space d'Alambertian. The 3+1 decomposition of the metric (14) in transverse-traceless gauge is

$$g_{ij} = f_{ij} + Ah_{ij}, \tag{16}$$

$$\beta^i = 0, \tag{17}$$

$$N = 1, \tag{18}$$

where f_{ij} denotes the flat spatial metric. From the evolution equation for g_{ij}, Eq. (2), we find the extrinsic curvature

$$K_{ij} = -\frac{A}{2}\dot{h}_{ij}. \tag{19}$$

The spacetime metric (14) satisfies Einstein's equations to first order in A. Consequently, (g_{ij}, K^{ij}) from Eqs. (16) and (19) will satisfy the constraints to linear order in A. Since we intend to increase A to order unity, this is not sufficient, and we must solve the constraint equations. Because the spatial metric, Eq. (16) and its time-derivative, $A\dot{h}_{ij}$, are known, it seems appropriate that this information be incorporated into the constraint-solve.

In light of the conformal thin sandwich formalism, it seems obvious to use Eq. (16) as conformal metric, and to base the time-derivative of the conformal metric on $\dot{h}_{ij}$:

$$\tilde{g}_{ij} = f_{ij} + Ah_{ij}, \qquad (20)$$

$$\tilde{u}_{ij} = A\dot{h}_{ij} - \frac{1}{3}\tilde{g}_{ij}\tilde{g}^{kl}A\dot{h}_{kl}. \qquad (21)$$

The second term in (21) ensures that $\tilde{u}_{ij}$ is trace free with respect to $\tilde{g}_{ij}$. Because h_{ij} and $\dot{h}_{ij}$ are traceless, Eq. (19) suggests the choice

$$K = 0. \qquad (22)$$

The free data is completed by setting

$$\partial_t K = 0. \qquad (23)$$

While the free data Eqs. (20)–(23) were motivated by a small perturbation, they can be used equally well for large amplitudes A (as long as solutions can be found). Hence, by increasing A, one can obtain nonlinearly perturbed initial data sets.

In writing down Eqs. (22) and (23), we have neglected terms of order $\mathcal{O}(A^2)$ on the right hand sides which arise because h_{ij} is traceless with respect to the flat metric f_{ij}, but not with respect to the perturbed metric $f_{ij} + Ah_{ij}$. Linearized gravity cannot determine such higher order terms. Since nonlinearities of Einstein's equations arise at the same order, and these nonlinearities are not accounted for in h_{ij}, we see no advantage to including $\mathcal{O}(A^2)$ terms in Eqs. (22) and (23). We have also chosen to use Eq. (23) as free data and include Eq. (13) as a fifth elliptic equation. An alternative is to set $\tilde{N} = 1$, and to solve only the four equations (8) and (9). Both alternatives are identical to linear order in A.

Equations (20)–(23), which result in a perturbation of Minkowski space, can be generalized to curved backgrounds easily by replacing the flat metric by a curved metric: Let g_{ij}^0 and K^0 be the 3-metric and mean curvature of an asymptotically flat, spatial slice through a stationary spacetime (for example flat space or a Kerr black hole). Solve the conformal thin sandwich Eqs. (8), (9), and (13) with the free data

$$\tilde{g}_{ij} = g_{ij}^0 + Ah_{ij}, \qquad (24)$$

$$\tilde{u}_{ij} = A\dot{h}_{ij} - \frac{1}{3}\tilde{g}_{ij}\tilde{g}^{kl}A\dot{h}_{kl}, \qquad (25)$$

$$K = K^0, \qquad (26)$$

$$\partial_t K = 0. \qquad (27)$$

We consider a few limiting cases

  (i) For $A = 0$ the free data reduce to $\tilde{g}_{ij} = g_{ij}^0$, $K = K^0$, $\tilde{u}_{ij} = \partial_t K = 0$. In this case, the underlying sta-

tionary spacetime is a solution of the conformal thin sandwich equations.
 (ii) For $A \ll 1$ and the wave h_{ij} located in the asymptotically flat region of the hypersurface, linear theory is valid. The properties of the perturbation in the initial data set will be precisely those of the underlying linear wave h_{ij}.
(iii) For large A we will have a nonlinearly perturbed spacetime, our primary interest. Because of the nonlinearity of Einstein's equations, the properties of such a strongly perturbed spacetime will differ from the linear wave. However, we expect that the qualitative properties are unchanged.

For constructing perturbed initial data on a curved background, one can, of course, also use a gravitational wave h_{ij} which represents a linear wave on the *background* g_{ij}^0, rather than on flat space. In that case, the $A \ll 1$ limit approaches the underlying linear wave even if the underlying wave is located in the strong field region. Since construction of linear waves on curved backgrounds is more complicated than on flat space, the decision whether this is necessary for a particular application will depend on how closely the perturbation must match an exact linear wave in the limit $A \ll 1$. Superposition of a flat space linear wave at intermediate separations from a black hole, say, $10M$ or $20M$, should result in a gravitational wave which predominantly, although not exactly, retains the properties of the linear wave, which may be sufficient for many applications.

Finally, we remark that our approach is related to and generalizes work by Abrahams and Evans [2,19], Shibata and Nakamura [20], and Bonazzola *et al.* [21]. Abrahams and Evans [2,19] assume axisymmety, and set a certain component of the extrinsic curvature (namely K_θ^r in spherical coordinates) equal to the value appropriate for the linear wave. Then they solve the momentum constraints for the remaining components of K_{ij}. This procedure singles out a preferred coordinate system, while our method is covariant with respect to spatial coordinate transformations.

Shibata and Nakamura [20] use the extrinsic curvature decomposition [24,25] to construct initial data, rather than the conformal thin sandwich equations. By choosing a maximal slice, $K = 0$, Hamiltonian and momentum equation decouple, and the momentum constraint is solved by the analytical (transverse trace free) extrinsic curvature determined from the underlying linearized wave. This is a very elegant approach, since only the Hamiltonian constraint remains to be solved for the conformal factor; however, decoupling of the Hamiltonian and momentum constraint happens only for slices with constant K. In order to construct perturbations of black hole spacetimes with nonconstant K, the coupled elliptic equations within the extrinsic curvature decomposition have to be solved. This

extension is conceptually straightforward and would lead to a method parallel to the one presented here, but using the extrinsic curvature decomposition rather than the conformal thin sandwich formalism.

Bonazzola *et al.* [21], finally, use the conformal thin sandwich formalism to superpose a time-symmetric linearized wave ($\partial_t \tilde{g}_{ij} = 0$, i.e., a superposition of an incoming and an outgoing wave) on flat space. This work employs Dirac-gauge and relies heavily on spherical coordinate systems in the reduction of the remaining degrees of freedom to two scalar functions. Our method, in contrast, can be used with any spatial coordinates, which is of particular importance for superposition of gravitational waves on black hole backgrounds, which may not be available in Dirac-gauge. Furthermore, while we use Teukolsky waves below as an example, our method can also be applied to different linearized waves, for example, a spherical wave superposed with a plane wave, which would be more difficult to implement in the approach taken in Ref. [21].

III. NUMERICAL RESULTS

A. Quadrupole waves

We illustrate the general method introduced in Sec. II with linearized quadrupole waves as given by Teukolsky [28]. This reference explicitly presents even parity waves, which are superpositions of $l = 0, 2$, and 4 modes, as well as odd parity waves, which are constructed as superpositions of $l = 1$ and 3. For each parity, there are five independent modes, corresponding to azimuthal quantum number $m = \pm 2, \pm 1, 0$. The even parity outgoing wave has a spacetime line-element

$$
\begin{aligned}
{}^{(4)}ds^2 &= -dt^2 + (1 + Af_{rr})dr^2 + (2Bf_{r\theta})rdrd\theta \\
&+ (2Bf_{r\theta})r\sin\theta drd\phi \\
&+ \left(1 + Cf_{\theta\theta}^{(1)} + Af_{\theta\theta}^{(2)}\right)r^2 d\theta^2 \\
&+ [2(A - 2C)f_{\theta\phi}]r^2 \sin\theta d\theta d\phi \\
&+ \left(1 + Cf_{\phi\phi}^{(1)} + Af_{\phi\phi}^{(2)}\right)r^2 \sin^2\theta d\phi^2.
\end{aligned} \tag{28}
$$

with radial dependence given by

$$
A = 3\left[\frac{F^{(2)}}{r^3} + \frac{3F^{(1)}}{r^4} + \frac{3F}{r^5}\right], \tag{29}
$$

$$
B = -\left[\frac{F^{(3)}}{r^2} + \frac{3F^{(2)}}{r^3} + \frac{6F^{(1)}}{r^4} + \frac{6F}{r^5}\right], \tag{30}
$$

$$
C = \frac{1}{4}\left[\frac{F^{(4)}}{r} + \frac{2F^{(3)}}{r^2} + \frac{9F^{(2)}}{r^3} + \frac{21F^{(1)}}{r^4} + \frac{21F}{r^5}\right], \tag{31}
$$

where

$$
F^{(n)} \equiv \left[\frac{d^n F(x)}{dx^n}\right]_{x=t-r}. \tag{32}
$$

$F(x) = F(t - r)$ describes the shape of the wave. The functions $f_{rr}, \ldots, f_{\phi\phi}^{(2)}$ depend only on angles (θ, ϕ); they are given explicitly in Ref. [28] for each azimuthal quantum number M. Ingoing quadrupole waves are obtained by replacing $F(t - r)$ with a function of $t + r$, and reversing the signs in front of odd derivatives of F in Eq. (32). Reference [28] gives also the metric for odd parity waves. From Eq. (28), one can easily extract h_{ij} and $\dot{h}_{ij}$.

B. Flat space with ingoing pulse

We consider a perturbation of flat space, $g_{ij}^0 = f_{ij}$, $K^0 = 0$. We choose the even parity, $m = 0$ ingoing mode. The shape of the pulse is taken as a Gaussian

$$
F(x) = e^{-(x-x_0)^2/w^2} \tag{33}
$$

of width $w = 1$ and with an initial radius of $x_0 = 20$.

Equations (8), (9), and (13) are solved with the pseudo-spectral elliptic solver described in [16]. The domain decomposition used in the elliptic solver is shown in Fig. 1. We use three spherical shells with boundaries at radii $r = 1.5, 16, 24$, and 10^9, so that the middle shell is centered on the gravitational wave. The inner shell does not extend to the origin, since the regularity conditions at the origin of a sphere are not implemented in the code. Instead, we place a cube on the origin which overlaps the innermost spherical shell. The solutions of the constraint equations turn out to be very smooth except for high frequency radial variations at the location of the gravitational wave pulse, cf. Eq. (33). Therefore, the accuracy is completely determined by the number N_r of radial basis functions in the middle spherical shell, which is chosen significantly larger than the number
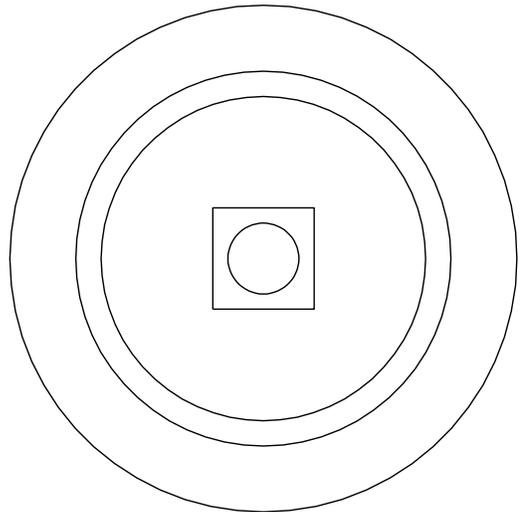

FIG. 1. Domain decomposition in R^3. A cube covers the central region which is not covered by the spherical shells.

of basis functions in the other subdomains. At the highest resolution, there are $N_r = 84$ radial basis functions in the middle shell, but only 28 in the other two shells. Furthermore, the angular resolution of all shells is $L = 15$ and the cube has 18 basis functions in each dimension.

Figure 2 presents the residuals of Hamiltonian and momentum constraints, Eqs. (4) and (5) for the linear gravitational wave *without* solving the constraints, i.e., upon direct substitution of Eqs. (16) and (19) into the constraint equations. As expected, the residual is $\mathcal{O}(A^2)$, confirming that the quadrupole wave is indeed a solution of linearized gravity.

We now solve the conformal thin sandwich equations with the free data (24)–(27) for different A, and compute the ADM energy for each solution,

$$E_{\text{ADM}} = \frac{1}{16\pi} \int_\infty (g_{ij,j} - g_{jj,i}) d^2 S_i. \tag{34}$$

Figures 3 and 4 plot the residual of the Hamiltonian constraint and the error of the ADM energy versus N_r. Exponential convergence is apparent, until roundoff limit is encountered around $\sim 10^{-10}$. The seemingly large value of this number (when compared to the usual double precision floating point accuracy of $\sim 10^{-17}$) is a consequence of the many numerically computed derivatives that enter the calculation: To compute $\tilde{R}$ in Eq. (4), second numerical derivatives of the conformal metric Eq. (16) are taken. After solution of the elliptic equations, the physical metric g_{ij} is assembled, and the Hamiltonian constraint Eq. (4) is evaluated using second numerical derivatives of g_{ij}. Each of these numerical differentiations increases the roundoff error by a factor of order the number of basis functions.
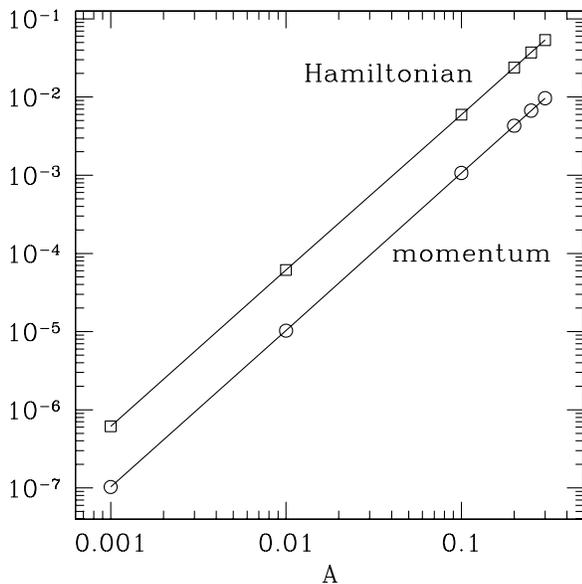

FIG. 2. Constraint violation of linear gravitational wave in flat background prior to solving the constraints.
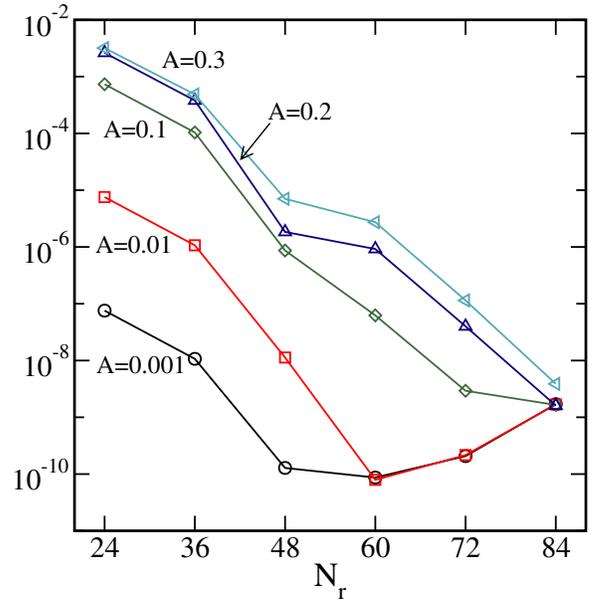

FIG. 3 (color online). Convergence of the elliptic solver for different amplitudes A. Plotted is the residual in the Hamiltonian constraint (root mean square) versus the number of radial basis functions in the middle spherical shell.

The increase in roundoff error with the number of basis functions can be clearly seen in Fig. 3

We now turn our attention from the convergence properties to the actual solutions of the constraint equations. For small A, we find that $\psi - 1$ is proportional to A^2
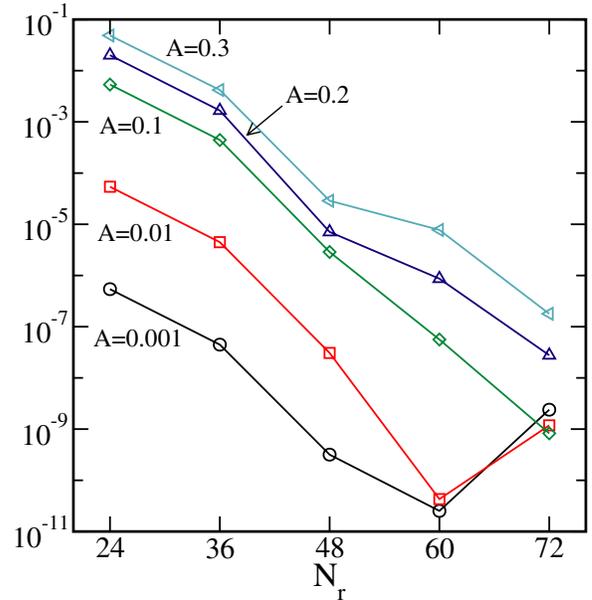

FIG. 4 (color online). Convergence of the elliptic solver for different amplitudes A. Plotted is the difference of the ADM energy to the next higher resolution solution versus the number of radial basis functions in the middle spherical shell.
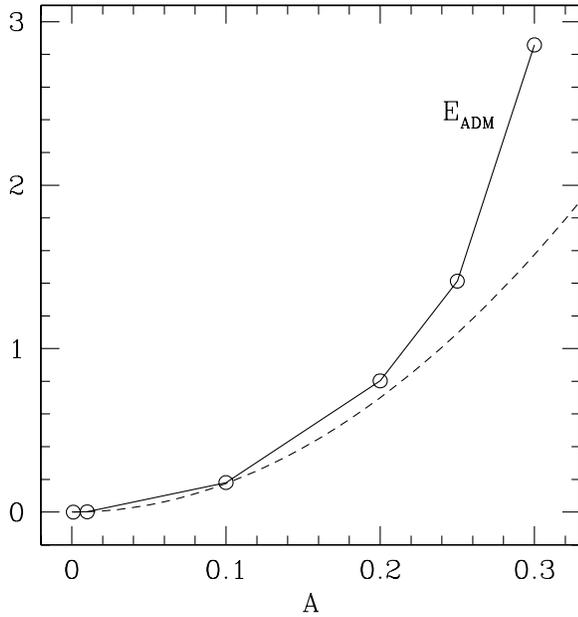
FIG. 5. ADM energy of an ingoing Gaussian pulse in flat space. The dashed line indicates the low-amplitude quadratic behavior.

everywhere. This is expected, because $\psi - 1$ corrects the conformal metric to satisfy the Hamiltonian constraint. As the constraint violation is proportional to A^2, so is this correction. Figure 5 proves that one can clearly achieve initial data sets with a significant energy content. At low amplitudes, E_{ADM} is proportional to A^2, as one expects given that $\psi - 1$ is proportional to A^2. At high amplitudes, however, E_{ADM} grows faster than A^2, indicating that the
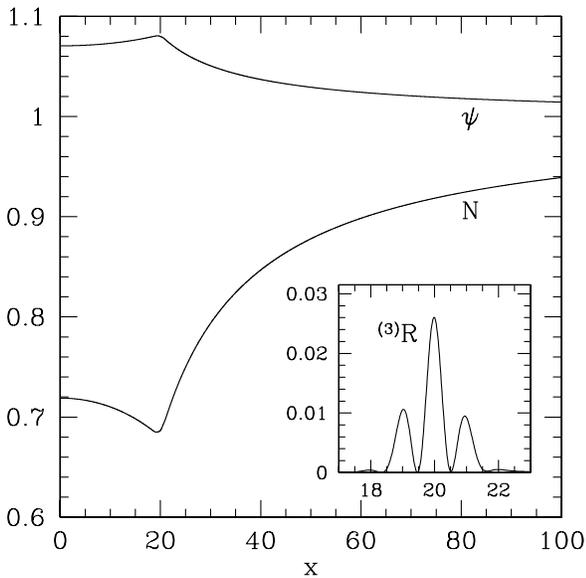

FIG. 6. Cuts through the equatorial plane of the $A = 0.3$ data set of Fig. 5. The large plot shows lapse and conformal factor, the inset shows the scalar curvature of the 3-metric.

nonlinear regime with self-interaction is reached. For $A > 0.3$, the elliptic solver fails to converge.

We now discuss the data set with amplitude, $A = 0.3$ in more detail. Its ADM energy is $E_{\text{ADM}} = 2.858$. Figure 6 presents cuts through the conformal factor ψ, lapse N and the scalar curvature of the physical 3-metric, $^{(3)}R$. Conformal factor and lapse deviate significantly from unity confirming that the solution is indeed deep in the nonlinear regime. The scalar curvature is virtually zero everywhere except within a spherical shell with $18 \lesssim r \lesssim 20$. Although the linearized wave is based on a Gaussian profile Eq. (33), even finer features are introduced into the linearized wave (and into the scalar curvature plotted in Fig. 6) because of the derivatives in Eqs. (29)–(31). Resolution of these fine features necessitates the high radial resolution of N_r.

The gravitational wave is concentrated in a spherical shell of width $w = 1$. The underlying *linear* wave is purely ingoing, so it seems reasonable that the gravitational perturbation in the physical, *nonlinear* spacetime is also predominantly ingoing. Neglecting dispersion, the wave will concentrate in a sphere centered at the origin with radius $r \sim w$. Black holes usually form for systems with mass to size ratio of order unity; here, $E_{\text{ADM}}/w \approx 2.8$, so that black hole formation appears very likely once the pulse is concentrated at the origin.

These data sets could be used to examine critical collapse to a black hole, repeating Abrahams and Evans [2] and extending it to genuinely three-dimensional collapse by choosing $m \neq 0$ in the underlying quadrupole wave. These data sets also provide a test bed for evolution codes in situations where the *topology* of the horizons changes.

C. Black hole with gravitational wave

As a second example of the flexibility of our method, we superpose a gravitational wave on a black hole background. The background spatial metric and trace of the extrinsic curvature are set to a Schwarzschild black hole in Eddington-Finkelstein coordinates,

$$g_{ij}^0 = \delta_{ij} + \frac{2M}{r} n^i n^j, \tag{35}$$

$$K_0 = \frac{2M}{r^2}\left(1 + \frac{2M}{r}\right)^{-3/2}\left(1 + \frac{3M}{r}\right), \tag{36}$$

where $n^i = x^i/r$, and $r^2 = \delta_{ij}x^i x^j$.

We choose an odd, ingoing $m = 0$ quadrupole wave with Gaussian shape, Eq. (33) at location $x_0 = 15$ and width $w = 1$. The metric is singular at the origin, therefore we excise at an inner radius of $1.5M$ (which is inside the horizon). At this inner boundary, we impose simple Dirichlet boundary conditions appropriate for the unperturbed black hole: $\psi = 1$, and $N = N_0$ and $\beta^i = \beta_0^i$, with lapse and shift for Eddington-Finkelstein given by
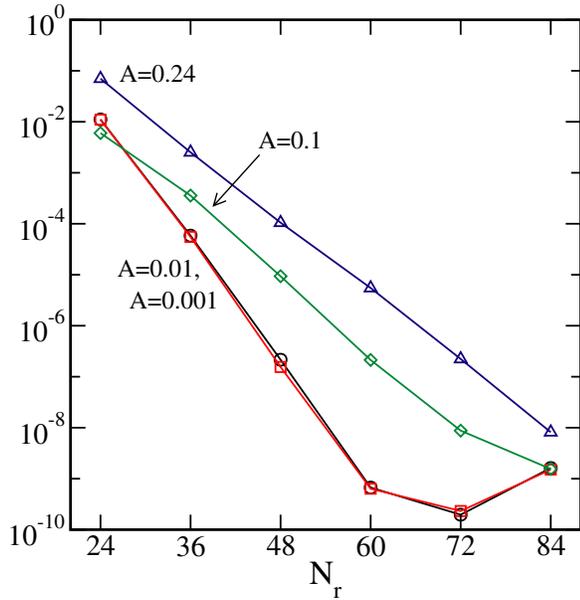
FIG. 7 (color online). Black hole with superposed gravitational wave: Residual of the Hamiltonian constraint versus radial number of basis functions in middle spherical shell.

$$N_0 = \left(1 + \frac{2M}{r}\right)^{-1/2}, \tag{37}$$

$$\beta_0^i = \left(1 + \frac{2M}{r}\right)^{-1} \frac{2M}{r} n^i. \tag{38}$$

Perturbed initial data sets are constructed for various values of A, and Fig. 7 demonstrates convergence of the solutions. In this case, the resolution is determined by two factors, namely, how well the gravitational wave is re-
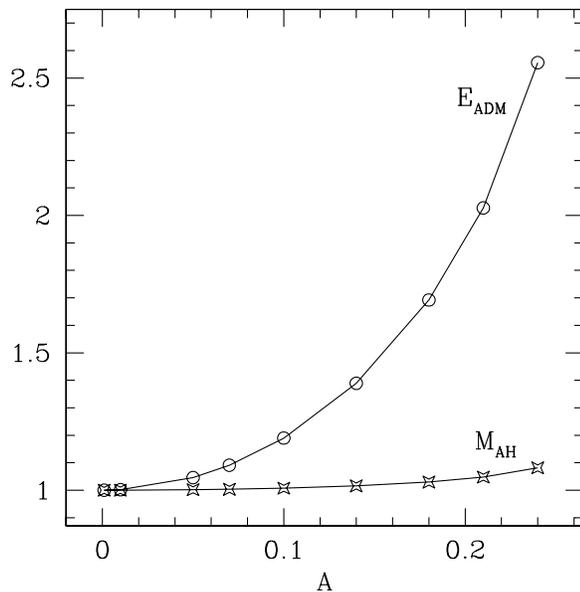
solved in the middle shell, and how well the inner shell resolves the background solution (g_{ij}^0, K_{ij}^0). For perturbations of Minkowski space, the latter was trivial (any expansion resolves the constant Minkowski background), however, here it is the limiting factor for small A or low resolutions, whereas for large A and high resolutions, both effects are about equally important. At the highest resolution, the number of radial basis functions in each shell is (from inner to outer) $48, 84$, and 28, and the angular resolution is unchanged from before, $L = 15$. In each resulting initial data set, the apparent horizon is located with the apparent horizon finder implemented and tested in [29–31], and the apparent horizon mass is computed from the area of the apparent horizon via

$$M_{\mathrm{AH}} = \sqrt{\frac{A_{\mathrm{AH}}}{16\pi}}. \tag{39}$$

Figure 8 presents the ADM energy and the apparent horizon mass of the central black hole as a function of the amplitude of the gravitational wave. The apparent horizon mass is fairly independent of A indicating that the horizon of the central black hole is only slightly perturbed by the gravitational wave. However, the ADM energy, which measures the total energy in the hypersurface, depends strongly on A; for large A,

$$\frac{M_{\mathrm{ADM}}}{M_{\mathrm{AH}}} \gtrsim 2.5, \tag{40}$$

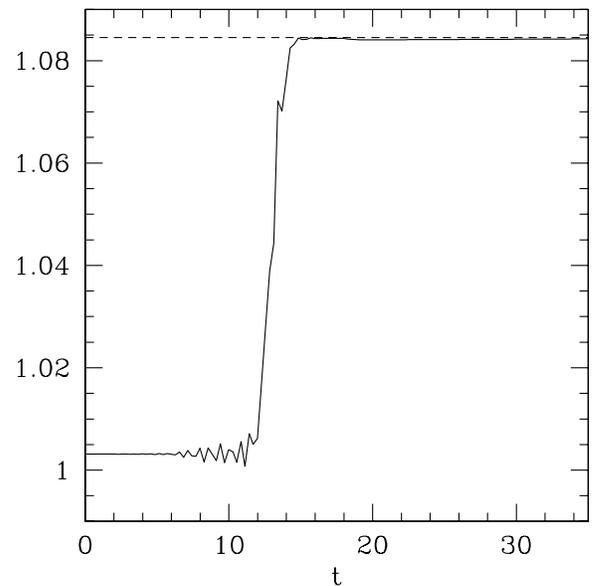FIG. 8. Black hole with superposed gravitational wave.

FIG. 9. Apparent horizon mass during an evolution of a perturbed black hole spacetime. The dashed line indicates E_{ADM} as computed from the initial data set.

indicating that a significant amount of gravitational energy resides outside the black hole.

To support our assertion that the superposed initial data set retains the features of the underlying gravitational wave, we present a preliminary evolution of a black hole with superposed ingoing gravitational wave [32]. The initial data for the evolution is identical to the data sets used in Fig. 8 with the one exception that the gravitational wave has even parity. Figure 9 shows the apparent horizon mass as a function of evolution time. All quantities are scaled such that the unperturbed Schwarzschild black hole has unit mass. For $t \lesssim 10$, M_{AH} is constant, its value being that from the initial data set. Between $12 \lesssim t \lesssim 15$, M_{AH} increases rapidly to an asymptotic value of $M_{AH}^f \approx 1.084$. The ADM energy of the initial data set was $E_{ADM} = 1.0845$. Apparently, the ingoing gravitational wave outside the black hole falls into it, increasing the area of the apparent horizon. The final apparent horizon mass is very close to the ADM energy, and the growth of M_{AH} happens during a time-interval comparable to the width of the initial pulse. Thus it appears that a large fraction of the wave is coherently ingoing and falls into the black hole.

IV. DISCUSSION

We propose a conceptually very clear method to construct spacetimes containing gravitational radiation which combines the conformal thin sandwich formalism with linear gravitational waves. For small amplitudes, the gravitational perturbation in the resulting initial data sets retains the characteristic features of the underlying linear wave, allowing for easy control of the properties of the gravitational wave perturbation. For strong amplitudes, nonlinearities of Einstein's equations are important, but we expect that the solutions still retain qualitatively the properties of the underlying linear wave.

To illustrate the method, we superpose quadrupolar gravitational waves onto Minkowski space, and onto a Schwarzschild black hole. In both cases, initial data with a large amount of gravitational energy in the perturbation can be constructed.

Numerically, these initial data sets provide test beds of evolution codes in situations away from stationarity. The mass of a central black hole changes—it may even double—when a large gravitational wave falls into it; can current gauge conditions handle this situation? If a gravitational wave collapses to a black hole, horizons appear, and evolution codes using black hole excision must accommodate this change. Furthermore, spacetimes with outgoing gravitational wave perturbations are ideal test beds for gravitational wave extraction algorithms, or constraint preserving boundary conditions [33].

Physically, ingoing gravitational wave pulses in Minkowski space, like the ones presented in Figs. 5 and 6, could be used to examine critical collapse, including the genuinely three-dimensional regime with $m \neq 0$. The black hole initial data sets with ingoing gravitational wave pulses (cf. Fig. 8) would be useful to examine scattering of the gravitational wave at the black hole [34–37]: What fraction of the gravitational wave is scattered and reaches infinity? Which multipole moments are excited in this process? This example can also be generalized to spinning black holes, off-centered gravitational waves, or gravitational waves with $m \neq 0$. Interesting questions in these scenarios would include, whether one can impart linear or angular momentum on the black hole.

ACKNOWLEDGMENTS

[1] M. W. Choptuik, Phys. Rev. Lett. **70**, 9 (1993).

[2] A. M. Abrahams and C. R. Evans, Phys. Rev. Lett. **70**, 2980 (1993).

[3] D. R. Brill, Ann. Phys. (N.Y.) **7**, 466 (1959).

[4] K. Eppley, Phys. Rev. D **16**, 1609 (1977).

[5] A. M. Abrahams, K. R. Heiderich, S. L. Shaprio, and S. A. Teukolsky, Phys. Rev. D **46**, 2452 (1992).

[6] D. Garfinkle and G. C. Duncan, Phys. Rev. D **63**, 044011 (2001).

[7] M. Alcubierre, G. Allen, B. Brügmann, G. Lanfermann, E. Seidel, W.-M. Suen, and M. Tobias, Phys. Rev. D **61**, 041501 (2000).

[8] S. R. Brandt and E. Seidel, Phys. Rev. D **54**, 1403 (1996).

[9] M. Shibata, Phys. Rev. D **55**, 7529 (1997).

[10] K. Camarda and E. Seidel, Phys. Rev. D **59**, 064019 (1999).

[11] J. Baker, S. Brandt, M. Campanelli, C. O. Lousto, E. Seidel, and R. Takahashi, Phys. Rev. D **62**, 127701 (2000).

[12] S. Brandt, K. Camarda, E. Seidel, and R. Takahashi, Classical Quantum Gravity **20**, 1 (2003).

[13] J. D. Brown and L. L. Lowe, Phys. Rev. D **70**, 124014 (2004).

[14] P. Marronetti and R. A. Matzner, Phys. Rev. Lett. **85**, 5500 (2000).

[15] P. Grandclément, E. Gourgoulhon, and S. Bonazzola, Phys. Rev. D **65**, 044021 (2002).

[16] H. P. Pfeiffer, L. E. Kidder, M. A. Scheel, and S. A. Teukolsky, Comput. Phys. Commun. **152**, 253 (2003).

[17] W. Tichy, B. Brügmann, M. Campanelli, and P. Diener, Phys. Rev. D **67**, 064008 (2003).

[18] C. W. Misner, K. S. Thorne, and J. A. Wheeler, *Gravitation* (W. H. Freeman, New York, 1973).

[19] A. M. Abrahams and C. R. Evans, Phys. Rev. D **46**, 4117(R) (1992).

[20] M. Shibata and T. Nakamura, Phys. Rev. D **52**, 5428 (1995).

[21] S. Bonazzola, E. Gourgoulhon, P. Grandclément, and J. Novak, Phys. Rev. D **70**, 104007 (2004).

[22] J. W. York, Jr., Phys. Rev. Lett. **82**, 1350 (1999).

[23] R. Arnowitt, S. Deser, and C. W. Misner, in *Gravitation: An Introduction to Current Research*, edited by L. Witten (Wiley, New York, 1962).

[24] J. W. York, Jr., in *Sources of Gravitational Radiation*, edited by L. L. Smarr (Cambridge University Press, Cambridge, England, 1979), p. 83.

[25] H. P. Pfeiffer and J. W. York, Jr., Phys. Rev. D **67**, 044022 (2003).

[26] L. Smarr and J. W. York, Jr., Phys. Rev. D **17**, 2529 (1978).

[27] J. R. Wilson and G. J. Mathews, in *Frontiers in Numerical Relativity*, edited by C. R. Evans, L. S. Finn, and D. W. Hobill (Cambridge University Press, Cambridge, England, 1989), pp. 306–314.

[28] S. A. Teukolsky, Phys. Rev. D **26**, 745 (1982).

[29] T. W. Baumgarte, G. B. Cook, M. A. Scheel, S. L. Shapiro, and S. A. Teukolsky, Phys. Rev. D **54**, 4849 (1996).

[30] H. P. Pfeiffer, S. A. Teukolsky, and G. B. Cook, Phys. Rev. D **62**, 104018 (2000).

[31] H. P. Pfeiffer, G. B. Cook, and S. A. Teukolsky, Phys. Rev. D **66**, 024047 (2002).

[32] L. E. Kidder and D. Shoemaker (private communication).

[33] L. E. Kidder, L. Lindblom, M. A. Scheel, L. T. Buchman, and H. P. Pfeiffer, gr-qc/0412116.

[34] G. Allen, K. Camarda, and E. Seidel, gr-qc/9806014.

[35] P. Papadopoulos, Phys. Rev. D **65**, 084016 (2002).

[36] Y. Zlochower, R. Gómez, S. Husa, L. Lehner, and J. Winicour, Phys. Rev. D **68**, 084014 (2003).

[37] D. Shoemaker, H. P. Pfeiffer, L. E. Kidder, and M. A. Scheel (to be published).